

# Finite Element Analysis of Fluid-Structure Interaction in Pressurized Tank Cars Subjected To Dynamic Impact Loading

Hailing Yu<sup>1</sup>, Yim Tang<sup>2</sup>, Jeffrey Gordon<sup>2</sup> and David Jeong<sup>2</sup>

<sup>1</sup> Chenega Advanced Solutions & Engineering, LLC, Cambridge, MA 02142, USA

<sup>2</sup> Volpe National Transportation Systems Center, Cambridge, MA 02142, USA

*Abstract: This paper presents a computational study of the fluid-structure interaction (FSI) mechanism in pressurized commodity tank cars in railroad application. Within the Lagrangian framework of Abaqus/Explicit, finite element analysis (FEA) is conducted to predict the structural response of tank cars under dynamic impact loading. A three-phase approach is adopted that explicitly models pressurized gas, pressurized liquid and tank car structure with three distinct sets of governing equations, and available contact options are investigated for modeling the interactions among different phases. To characterize the elastic-plastic behavior of a tank car structure, shell element formulation provides accurate solutions at relatively low costs. To capture the progressive fracture behavior of an impact zone, however, solid element formulation must be employed. The solid-to-shell coupling technique is employed in the latter case to avoid the high cost of an all-solid-element structural model. With small to moderate amounts of fluid sloshing in an impacted tank car, the general contact option is successful in simulating the FSI when the structural model involves only shell elements, whereas combined general contact and contact pair definitions are necessary if the structural model includes both shell and solid elements and solid-to-shell coupling. The force-displacement results from FEA show good correlations with the available shell (or side) impact test data.*

*Keywords: Railroad commodity tank car, pressurized tank car, shell impact, fluid-structure interaction, plastic deformation, fracture, finite element analysis, multi-phase simulation, ideal gas, equation of state, general contact, contact pair, and solid-to-shell coupling.*

## 1. Introduction

Pressurized commodity tank cars are commonly employed in railroad industry to transport liquefied goods including hazardous materials (hazmat) such as compressed flammable (e.g., propane) or toxic gases (e.g., chlorine). Severe impacts from accidents can compromise the structural integrity of a tank car and lead to serious safety, economic and environmental consequences. Thus improving the structural integrity of railroad tank cars carrying hazmat is of great importance, and it requires improved tank car designs as well as a better understanding of the dynamic mechanisms of involved constituents and their interactions. To achieve these goals,

computational methods such as finite element analysis (FEA) have proven to be a powerful tool that complements experimental approaches.

Under normal operating conditions, both liquid and vapor forms of a substance being transported coexist in a tank car. The pressure of a gaseous vapor in dynamic equilibrium with its liquid form at a given temperature is called a vapor pressure. Figure 1 shows the vapor pressures of water and chlorine over a range of temperatures. While vapor pressures of water appear to be negligible at normal temperatures, those of chlorine are more significant. Therefore, in a chlorine tank car there exist three interacting phases: solid structure, liquid and gas, as illustrated in Figure 2. The liquid and gas phases are also referred to as fluid phases.

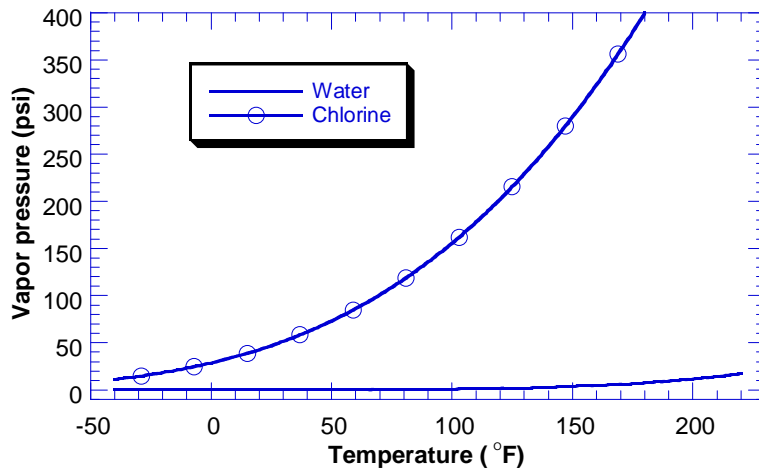


Figure 1. Vapor pressures of water and chlorine as functions of temperature<sup>1</sup>.

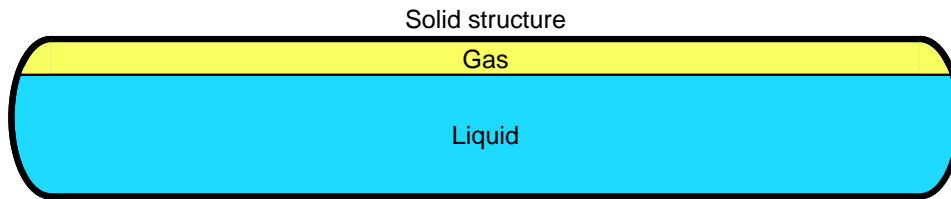


Figure 2. Illustration of solid, liquid and gas phases comprising a loaded tank car.

A tank car structure responds to external impact loading with elastic-plastic deformations that can ultimately stretch to a state of failure. In a tank car with liquefied lading such as chlorine, the fluid pressure also transmits to the inner wall and balances with the internal forces of the tank container. This is a typical fluid-structure interaction (FSI) phenomenon because the fluid pressure affects

<sup>1</sup>Vapor pressure  $P$  is calculated according to Antoine equation  $\ln(P)=A-B/(T+C)$ , where  $T$  is temperature and  $A$ ,  $B$  and  $C$  are Antoine coefficients from <http://www.cheresources.com/data.xls>.

the structural deformation and vice versa. Simplified computational approaches avoid explicitly modeling one or both fluid phases by replacing them with prescribed, constant inner wall pressure and/or lumped fluid mass. This may lead to inaccurate results when strong FSI effects are present. Therefore, a more realistic computational model of a loaded tank car should include multiple phases: solid structure, pressurized liquid and pressurized gas.

This paper presents a computational study of the multi-phase interactions in a tank car during a dynamic event. Provided that the degree of fluid sloshing is small to moderate, the FSI problem is solvable within the Abaqus Lagrangian framework. The paper is organized as follows. First, shell (or side) impact tests on full scale tank cars are described. Second, a computational multi-phase approach is presented. Third, the computational method is applied in simulating the shell impact tests and the simulation results are verified with the experimental data. Finally, conclusions are drawn from the study, and additional applications of the method are discussed.

## 2. Experimental study

The main structure of a tank car consists of two ellipsoidal ends (or heads) connected by a cylindrical shell. An object hits anywhere on the shell in a shell impact scenario, and it hits anywhere on the heads in a head impact scenario. Head impact tests on full-scale tank cars were conducted in the 1970's, whereas head component tests were done more recently. In 2007 full-scale shell impact tests were conducted at the Transportation Technology Center in Pueblo, Colorado. Results from these tests can help to develop and verify computational models as well as evaluate crashworthiness performance of existing tank cars.

Figure 3 shows typical tank and ram cars used in the shell impact tests in Pueblo, Colorado. For apparent safety reasons the tank car was filled with water in lieu of liquid chlorine to 89.4% of its capacity (i.e., 10.6% outage). In addition, clay slurry was added in the water and the mixture had the approximate density of liquid chlorine. Air occupied the rest of the tank volume and was pressurized to 100 psi to mimic the condition in a tank car loaded with liquid chlorine. The tank car assembly weighed about 263,000 pounds with its liquid content, a steel jacket and other accessories. It was placed with one side against a concrete wall and the other side exposed to impact from the ram car. The ram car was a ballasted flatcar that weighed 286,000 pounds and had a protruding beam to which an impactor was attached. Two impactors were employed in the shell impact tests, and their surface geometries are illustrated in Figure 4. Impactor I had a 17"×23" face (approximately the size of a draft sill cross-section) whose edges were rounded with 1" radius, and Impactor II had a 6"×6" face (approximately the size of a coupler shank cross-section) whose edges were rounded with 0.5" radius.

Among the instrumentations, accelerometers on the ram car yielded data to calculate impact forces and impactor displacements. Displacement transducers were mounted on the interior tank wall and provided tank indentation data. Pressure transducers were also placed on the interior tank wall to monitor the liquid pressure on selected locations (but no data channel monitored the air pressure).

An assurance test was first conducted with limited instrumentation, followed by two fully instrumented tests (Test 1 and Test 2). Impactor I was employed in Test 1 and Impactor II in Test

2. In both tests, the ram car ran the impactor perpendicularly to the center of the tank shell with an initially gained velocity (14 mph in Test 1 and 15.1 mph in Test 2). The tank car was dented 26 inches but maintained its structural integrity in Test 1. The tank car was punctured and the fluids escaped in Test 2. The peak force reached about 1290 kips in Test 1 and 910 kips in Test 2.



**Figure 3. Tank and ram cars in a shell impact test.**

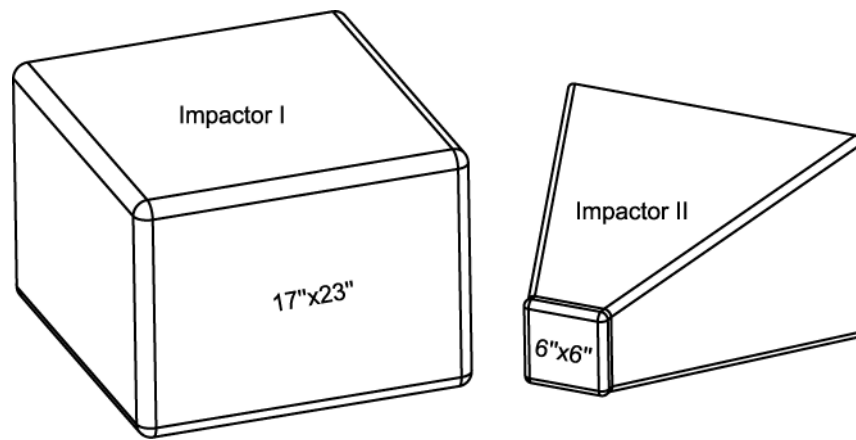


**Figure 4. Schematic of Impactor surfaces.**

### **3. Three-phase finite element model**

Finite element models are developed to simulate the tests described above. In one simplified approach the gas phase was omitted and the fluid pressure was replaced with a prescribed, constant pressure imposed on the inner wall of the tank container. This approach is quite accurate when the structural deformation is small or localized and thus has minimal effect on the fluid pressure. However, when the structural deformation becomes more influential over a larger domain and the FSI effect becomes more significant, this approach can be inaccurate. Another approach further omitted the liquid phase and distributed the liquid mass in the tank wall. In this

study, as described in the following subsections, all of the solid, liquid and gas phases following different sets of governing equations are explicitly modeled and their interactions accounted for via available contact options.

### 3.1 Governing equations

#### 3.1.1 Solid structure

The tank car structure is made of specialty steel such as TC-128B. The behavior of this solid structure phase is modeled with elastic-plastic and fracture constitutive laws. The elastic behavior is assumed to be linear and isotropic with Young's modulus  $E$  and Poisson's ratio  $\nu$ . Once the elastic limit is reached, a modified Ramberg-Osgood strain hardening law is followed

$$\varepsilon = \sigma/E + (\sigma/K)^n \quad (1)$$

where  $\varepsilon$  and  $\sigma$  are true strain and true stress, respectively, and  $n$  and  $K$  are material constants to be determined from material parameters such as the initial yield strength  $\sigma_{y0}$ .

As the yield stress evolves to its peak level, fracture or damage is assumed to initiate at an equivalent plastic strain  $\bar{\varepsilon}^{pl} = \bar{\varepsilon}_0^{pl}$ , which can be a function of stress triaxiality, strain rate, temperature, etc. This study adopts a fracture initiation criterion dependent on the stress triaxiality  $\eta$ , which is defined as the ratio of the hydrostatic mean stress ( $\sigma_m$ ) to the von Mises equivalent stress ( $\bar{\sigma}$ )

$$\eta = \sigma_m / \bar{\sigma} \quad (2)$$

where

$$\sigma_m = \frac{1}{3}(\sigma_1 + \sigma_2 + \sigma_3) \quad (3)$$

$$\bar{\sigma} = \sqrt{\frac{1}{2}[(\sigma_1 - \sigma_2)^2 + (\sigma_2 - \sigma_3)^2 + (\sigma_3 - \sigma_1)^2]} \quad (4)$$

A fracture locus can be constructed in the  $(\eta, \bar{\varepsilon}_0^{pl})$  plane from a fracture initiation criterion for a particular material. A three-branch fracture locus similar to that calibrated by Lee and Wierzbicki (2004) for industrial aluminum and steel is adopted here and expressed as

$$\bar{\varepsilon}_0^{pl} = \begin{cases} \infty, & \eta \leq -1/3 \\ C_1/(1+3\eta), & -1/3 < \eta \leq 0 \\ C_1 + (C_2 - C_1)(\eta/\eta_0)^2, & 0 \leq \eta \leq \eta_0 \\ C_2 \eta_0/\eta, & \eta_0 \leq \eta \end{cases} \quad (5)$$

where  $C_1$  is  $\bar{\varepsilon}_0^{pl}$  in pure shear ( $\eta=0$ ), and  $C_2$  is  $\bar{\varepsilon}_0^{pl}$  in uniaxial tension where  $\eta=\eta_0=1/3$ . The fracture locus derived from this expression is plotted in Figure 5: Branch I for ductile fracture due to the mechanism of void nucleation, growth and coalescence; Branch III for shear decohesion fracture; and Branch II for mixed mode fracture.

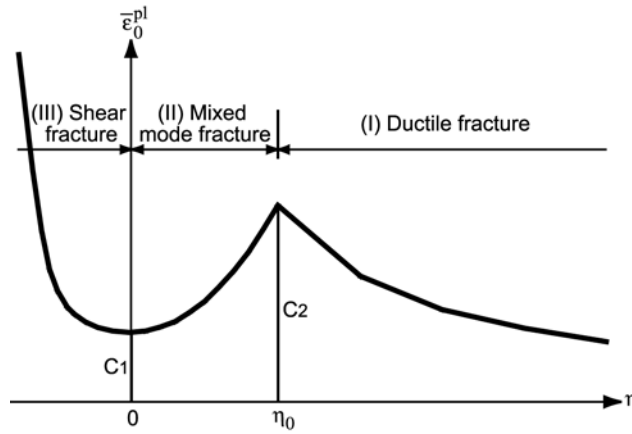


**Figure 5. Three-branch fracture initiation locus for industrial aluminum or steel.**

Abaqus has a progressive damage and failure model that accommodates the material behavior described above. With a predefined fracture initiation criterion  $\bar{\varepsilon}_0^{pl} = \bar{\varepsilon}_0^{pl}(\eta)$ , Abaqus determines that damage initiates if the following condition is met

$$\omega_D = \int \frac{d\bar{\varepsilon}_0^{pl}}{\bar{\varepsilon}_0^{pl}} = 1 \quad (6)$$

where  $\omega_D$  is a state variable that increases monotonically with plastic deformation. Abaqus assigns this implementation to the ductile fracture category, but as long as a fracture initiation criterion is defined over the entire stress triaxiality range  $(-\infty, +\infty)$ , this implementation seems applicable to shear and mixed mode fractures as well.

With the onset of damage, the yield stress softens and the elastic modulus degrades until the equivalent plastic strain reaches its failure state at  $\bar{\varepsilon}_f^{pl}$ . This damage evolution is monitored by an overall damage variable  $D$  which starts at 0 when  $\omega_D$  reaches 1 and progresses to 1 at complete failure. Abaqus allows various damage evolution forms and for simplicity, this study adopts a linear softening law. To reduce the mesh dependency inherent in softening responses, the concept of an element characteristic length is introduced in the constitutive relation and denoted as  $L_c$ . Further, an equivalent plastic displacement  $\bar{u}^{pl}$  is defined and evolves according to the following equation

$$\dot{\bar{u}}^{pl} = L_e \dot{\bar{\epsilon}}^{pl} \quad (7)$$

When  $\bar{u}^{pl}$  reaches  $\bar{u}_f^{pl}$  upon complete failure, elements representing failed material points can be removed from a model.

The thickness dimension of a tank car is considerably smaller than the other dimensions such as the tank diameter and length. Previous studies have established that to capture pure elastic-plastic behavior, shell element formulation is accurate with a typical element size of about  $2t$ , where  $t$  is tank thickness. For progressive damage and failure behavior, shell element formulation can produce misleading results and therefore, solid element formulation must be employed. Multiple layers of solid elements through the thickness are needed in this case to accurately capture the progressively deteriorating process. However, an all-solid-element model of a tank car is both expensive and unnecessary, and the solid-to-shell coupling technique in Abaqus can be employed instead. That is, the impact zone is modeled with multi-layered solid elements, the rest of the domain is modeled with shell elements, and the two domains are joined by solid-to-shell coupling.

### 3.1.2 Liquid phase

Hydrostatic behavior of the liquid phase is governed by equations of state that determine the pressure  $p$  (positive in compression) as a function of the density  $\rho$  and the specific energy  $E_m$  (internal energy per unit mass)

$$p=f(\rho,E_m) \quad (8)$$

The Mie-Grüneisen equation of state available in Abaqus/Explicit is linear in energy and can be written in the following form

$$p=f_1(\rho)+f_2(\rho)E_m \quad (9)$$

where  $f_1(\rho)$  and  $f_2(\rho)$  are model-dependent functions of density. A linear  $U_s-U_p$  Hugoniot form of the Mie-Grüneisen equation of state is an effective method to model the behavior of water or liquid chlorine. For this model, initial density  $\rho_0$  and wave speed  $c_0$  (from which  $\rho_0 c_0^2$  yields the elastic bulk modulus) are required material inputs.

Deviatoric behavior of the liquid phase is assumed to be uncoupled from its volumetric response and governed by either a linear isotropic elastic model or a Newtonian viscous fluid model. The shear viscosity parameter serves as a penalty to suppress shear modes that can distort a mesh and must be small for water which is inviscid.

### 3.1.3 Gas phase

The gas phase is assumed to follow the ideal gas equation of state

$$pV=mRT \quad (10)$$

where  $p$  is the absolute pressure,  $V$  is the volume,  $m$  is the mass,  $R$  is the (specific) gas constant and  $T$  is the absolute temperature. The gas constant  $R$  is a required input for this model. The ideal gas assumption is approximately true for the conditions considered. If there is no leakage or temperature change, the gas pressure is inversely proportional to the volume that the gas occupies, which apparently changes with structural deformation. It is assumed that the liquid and gas phases are in dynamic equilibrium and that temperature is constant throughout the process.

### **3.2 Modeling fluid-structure interaction**

In the experimental study described above, only small to moderate fluid sloshing is believed to have occurred, and the same is assumed in the modeling approach. Under this assumption, mesh distortion due to material flow is expected to be moderate at most, and the Lagrangian framework is applied. In applications with more significant fluid sloshing, the coupled Eulerian-Lagrangian (CEL) capability in Abaqus may be employed.

In addition to each individual phase, the interactions among different phases need to be addressed. Generally these interactions are analyzed as inter-phase contacts. The general contact option provides a robust solution to solid-to-liquid contacts. However, contacts involving the gas phase can be more problematic because its mass is extremely small compared to those of the other phases.

The gas-to-liquid interface is usually modeled with no separation, no slip contact, as is the CEL treatment of fluid interfaces. This is equivalent to firmly attaching two materials along their interface. Alternatively, such contact can be replaced with shared nodes along the interface to achieve the same modeling effect while eliminating a potential source of numerical instability – contacts between two materials vastly mismatched in mass. The choice of either option depends on the specific application and the desired performance.

To model the gas-to-solid interaction, general contact works well when the structural model includes only shell elements. However, when solid-to-shell coupling is involved, numerous trials led to the conclusion that contact pair between gas and solid phases must also be defined. In addition, it is helpful to define smooth contact surfaces for the fluids and zero contact thickness for shell elements. Frictionless contact is assumed for all fluid-to-fluid and fluid-to-structure interfaces.

## **4. Verification with experimental data**

The next step is to simulate the shell impact tests within the FEA framework described above and verify the computational results with the corresponding experimental data. The materials and geometries of the tank cars involved in the tests and the initial fluid pressure are summarized in Table 1. Like its physical counterpart, the tank car model consists of a cylindrical shell with two ellipsoidal heads. The only other structural entity that is explicitly modeled is the jacket, which has a clearance of about four inches from the exterior tank body. All the accessories are lumped into point masses. The model parameters for the steel materials are summarized in Table 2. As in the tests, the tank car model is filled with liquid for 89.4% of its volume and gas for 10.6% of its volume. The model parameters for liquid and gas phases are shown in Table 3. The liquid

properties are derived from those of the clay slurry-water mixture and liquid chlorine, and the gas properties are those of air. The initial fluid pressure  $p_0$  is implemented as an initial hydrostatic stress state ( $\sigma_{11}=\sigma_{22}=\sigma_{33}=-p_0$ ,  $\sigma_{12}=\sigma_{23}=\sigma_{31}=0$ ) for the three-dimensional fluid elements. The ram car is modeled as one of the impactor surfaces shown in Figure 4 with a lumped mass of 286,000 pounds.

**Table 1. Materials, geometries and initial condition of tank cars in the tests.**

Tank material	Inner diameter (inch.)	Head thickness (inch.)	Shell thickness (inch.)	Shell length (inch.)	Jacket material	Jacket thickness (inch.)	Initial fluid pressure (psi)
TC-128B	100.75	0.828	0.777	471.47	ASTM A1011/A569	0.119	100

**Table 2. Model parameters for tank car materials.**

Material	$\rho$ (lbm-in <sup>-3</sup> )	$E$ (ksi)	$\nu$	$\sigma_{y0}$ (ksi)	$n$	$K$ (ksi)	$C_1$	$C_2$	$\bar{u}_f^{pl}$ (inch.)
TC-128B from Test 1	0.2835	29800	0.3	55	10.55	99.15	-	-	-
TC-128B from Test 2	0.2835	31650	0.3	55	11.17	96.04	0.31	1.05	0.32
ASTM A1011/A569	0.2835	29000	0.3	30	9.00	59.85	0.31	0.92	0.25

**Table 3. Model parameters for liquid and gas phases.**

Material	$\rho_0$ (lbm-in <sup>-3</sup> )	$c_0$ (in-sec <sup>-1</sup> )	$R$ (in <sup>2</sup> -sec <sup>-2</sup> -K <sup>-1</sup> )
Liquid	0.0510	34732.95	-
Gas	0.0003	-	479034.86

#### 4.1 Elastic-plastic and FSI analysis

To simulate shell impact Test 1, only shell elements and elastic-plastic material models are employed, because the structural integrity was maintained as a result of the impact test. Modeling FSI is straightforward in this case with one general contact definition. The calculated mass of the tank car assembly is 268,656 pounds, within 2.2% of the nominal 263,000 pounds. The problem domain, boundary conditions and loading are assumed to be symmetric about the center transverse section, so a half-symmetric model illustrated in Figure 6 is developed. In addition to the components described above, Figure 6 shows a rigid wall (fixed in space) and a rigid lower support (attached to the tank assembly and prevented from downward movements by a fixed rigid floor not shown in the picture) that approximate the test conditions. As initial conditions, the impact mass moves at a speed of 14 mph toward the stationary tank assembly.

The following analysis results are compared with the experimental data: impact force ( $F$ , Figure 7a) and impactor displacement ( $d$ , Figure 7b) along the impact direction;  $F$ - $d$  cross plot (Figure 7c); tank indentation measured at the center cross-section ( $d_i$ , Figure 7d); and work done by the impact force or integration of the  $F$ - $d$  curve ( $W$ , Figure 7e). All of these analysis results show good correlations with the experimental data.

In addition, the pressure time history averaged over all gas elements (denoted as  $p_{gas}$ ) is extracted from Abaqus and plotted in Figure 7(f) (the corresponding test data is not available). Because

initial gaps exist between the inner tank wall and the fluid surfaces in the model definition, to close the gaps the fluids experience an initial volume expansion which causes an initial drop in the fluid pressure. To mitigate this effect, an initial fluid pressure slightly larger than  $p_0$  is assigned (101 psi in this case as determined from several iterations). Figure 7(f) indicates that within 6 milliseconds the gas pressure already drops to and stays steady at around 100 psi. The gas pressure reaches a maximum of 135 psi near 0.216 seconds.

To help understand the impact mechanisms involved in Test 1, five deformation/contact states are identified from the simulation and highlighted on the  $F-d$  curve in Figure 8. Initially the impactor contacts with the jacket only (State A). As the impactor pushes further, the jacket gets in contact with the exterior tank surface and the force reaches its first peak around State B. At State C the tank surface on the other side reaches against the rigid wall along with the jacket, and the force starts to climb up again. This contact state lasts to the point that the maximum tank indentation is reached around the second peak force (State D). The impact mass loses its forward moving momentum from this point on and starts to rebound from the tank assembly which in turn rebounds from the rigid wall. At State E the rebound process is complete with the solid entities separated from each other.

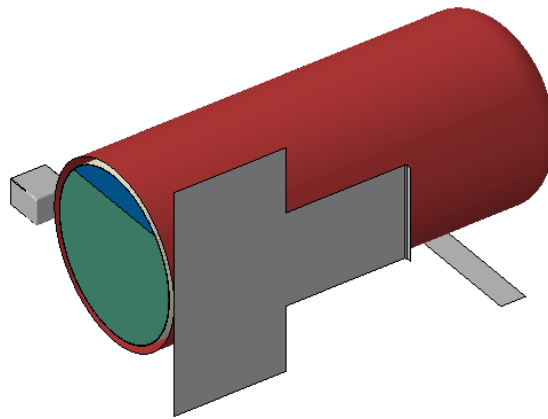


**Figure 6. Half symmetric model for shell impact Test 1.**

#### **4.2 Fracture and FSI analysis**

In shell impact Test 2 the tank car was breached with the use of a smaller impactor (Impactor II in Figure 4). The impact mass had a greater initial speed (15.1 mph). The progressive damage and failure material model is applied to the solid elements in the tank car's impact zone which transition to shell elements via solid-to-shell coupling. The tank car assembly weighs 264,756 pounds in the model. In addition to the general contact definition, a contact pair definition addresses the solid-to-gas interaction. Figure 9(a) shows the final damage profile from Test 2, and Figure 9(b) shows model predicted damage at 0.104 seconds (when elastic deformations are not yet recovered and the cutout specimen shows a concave shape instead of the convex shape in Figure 9a). The simulation was stopped at this point because the failed structure can no longer contain the fluids.

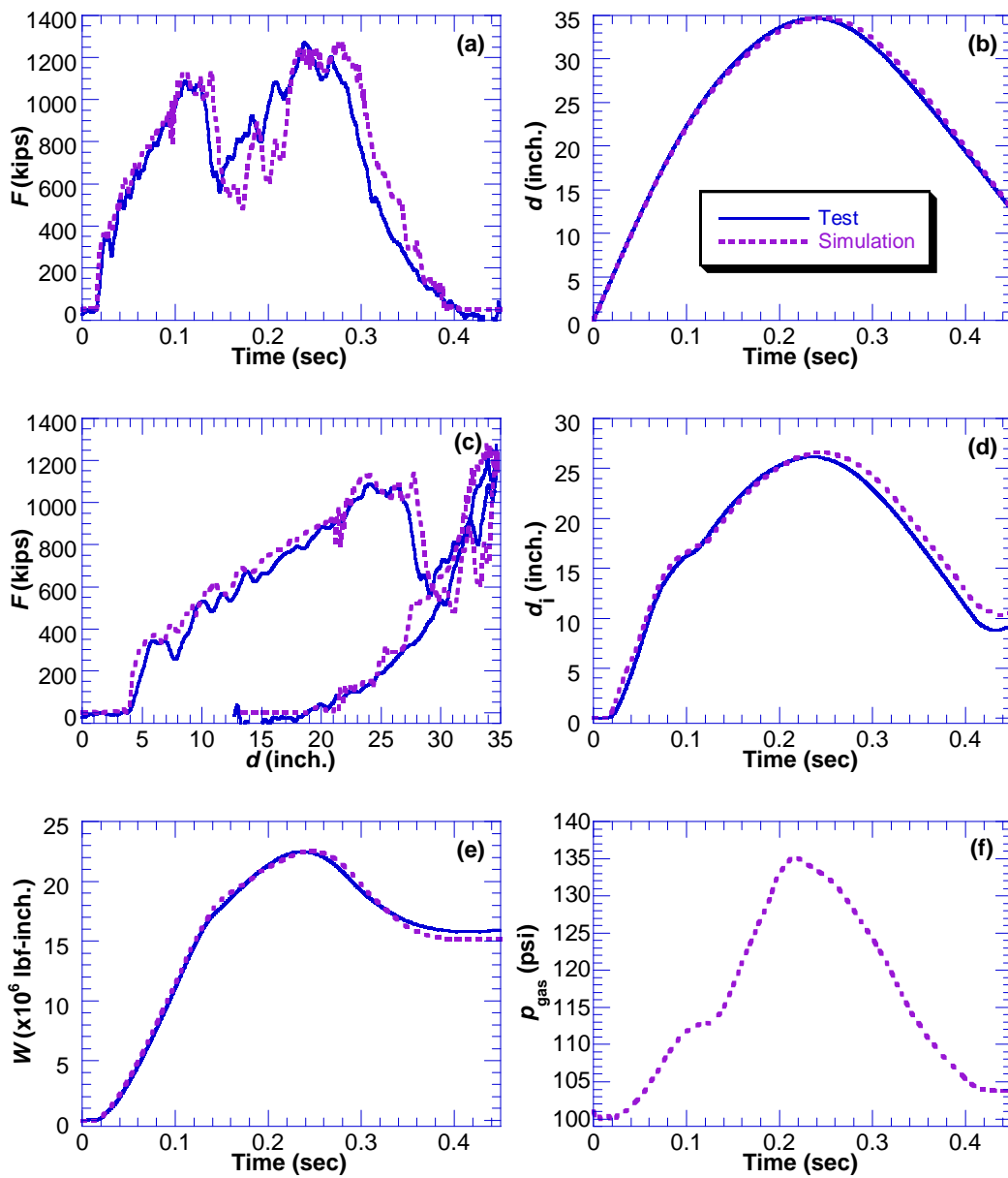
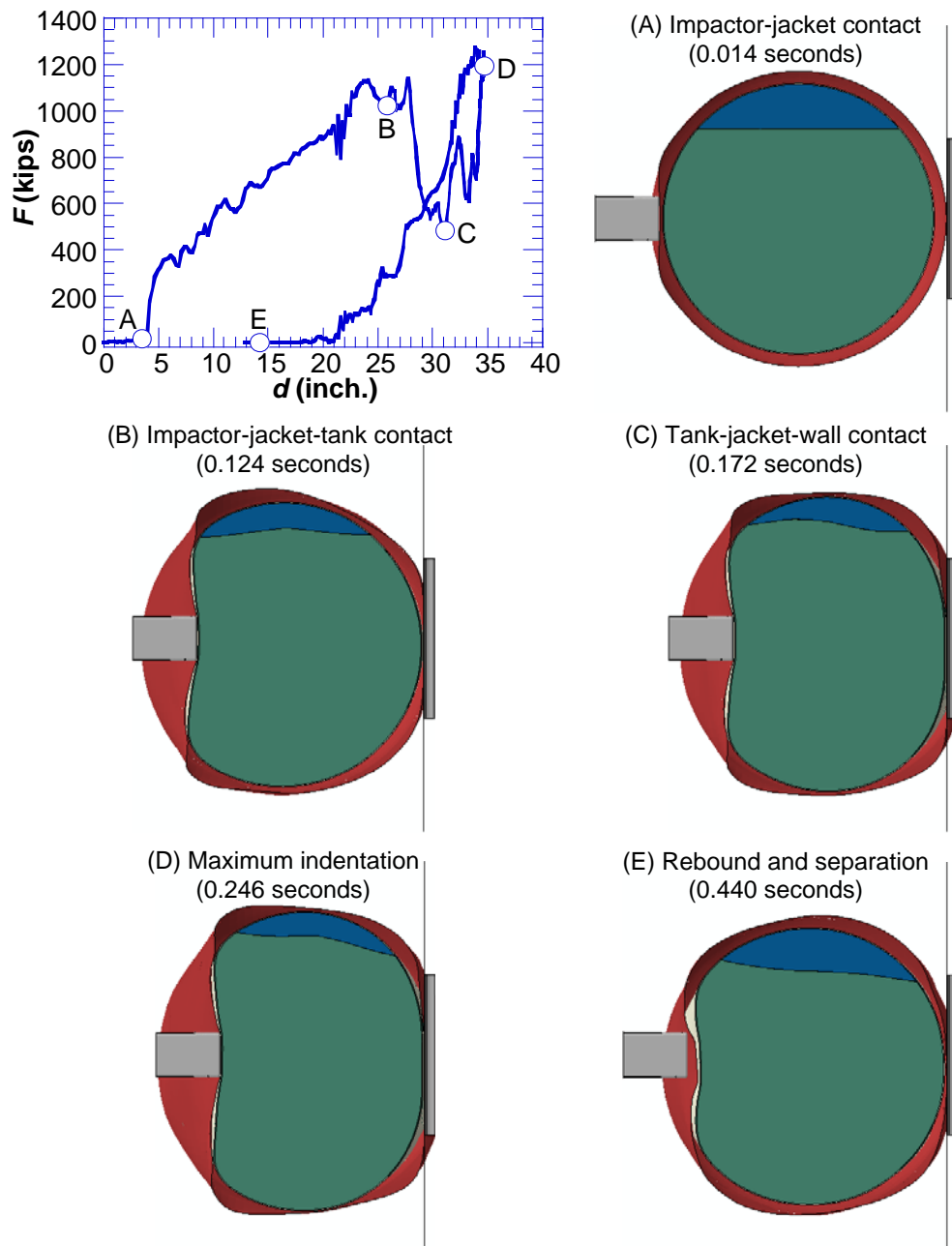
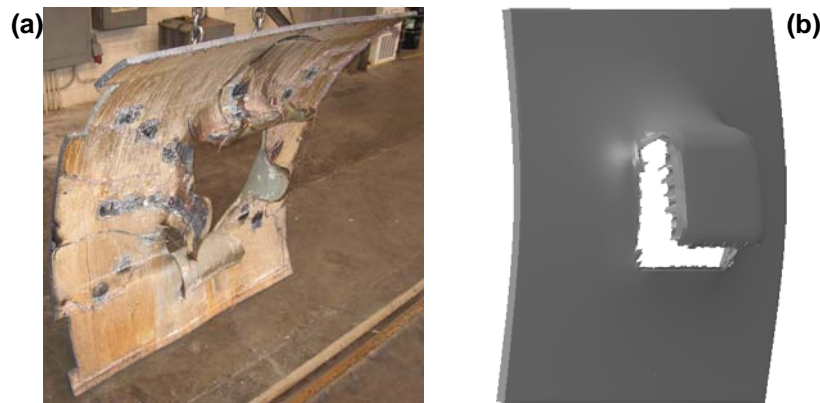


Figure 7. Analysis vs. test results for shell impact Test 1: (a) impact force  $F$ , (b) impactor displacement  $d$ , (c)  $F-d$  cross plot, (d) tank indentation  $d_t$ , (e) work  $W$  done by impact force, and (f) gas pressure  $p_{\text{gas}}$  (analysis data only).



**Figure 8. Five deformation/contact states identified from the simulation of shell impact Test 1.**



**Figure 9. Damage profile from (a) test, and (b) simulation (at 0.104 seconds) of shell impact Test 2.**

Figures 10(a-e) compares the calculated impact force  $F$ , impactor displacement  $d$ ,  $F-d$  cross plot, tank indentation  $d_i$  and work  $W$  done by the impact force with the corresponding test data. Again good correlations are observed. The sudden drop in force near 0.1 seconds in Figure 10(a) indicates the breach of the tank car. The simulation predicts well both the timing of this event and the maximum force level. The work done by impact force shown in Figure 10(e) indicates that it takes the energy of nearly 12 million lbf-inch to break the tank car under the specific test set up, and this translates to a minimum puncture velocity of nearly 10 mph for a 286,000 pound ram.

Figure 10(f) shows the gas pressure  $p_{\text{gas}}$  over time from the simulation. The initial gas pressure is set at 110 psi which quickly drops to around 100 psi as a result of the initial volume expansion. The gas pressure reaches a maximum of 110 psi right before the tank car breach. This pressure level implies that the FSI effect was weaker in Test 2 than it was in Test 1.

## 5. Conclusions and discussions

A computational method within the Lagrangian framework of Abaqus/Explicit was developed and applied in simulating two shell impact tests on full-scale tank cars. The simulations predicted force, displacement and work time histories in good agreement with those recorded in the tests. It demonstrated that the presented computational approach is effective and accurate in depicting the elastic-plastic material behavior, progressive damage and failure process and fluid-structure interaction mechanism within an impacted tank car.

The same approach can be useful in several other tank car applications. It can be employed to determine the minimum impact energy needed to puncture a tank car under given test conditions. Although shell impact scenarios were used to verify the method, it can be similarly applied to head impact scenarios as long as fluid sloshing does not cause excessive mesh distortion. Finally the computational approach can help to accurately evaluate the benefits of improved protective strategies for tank cars.

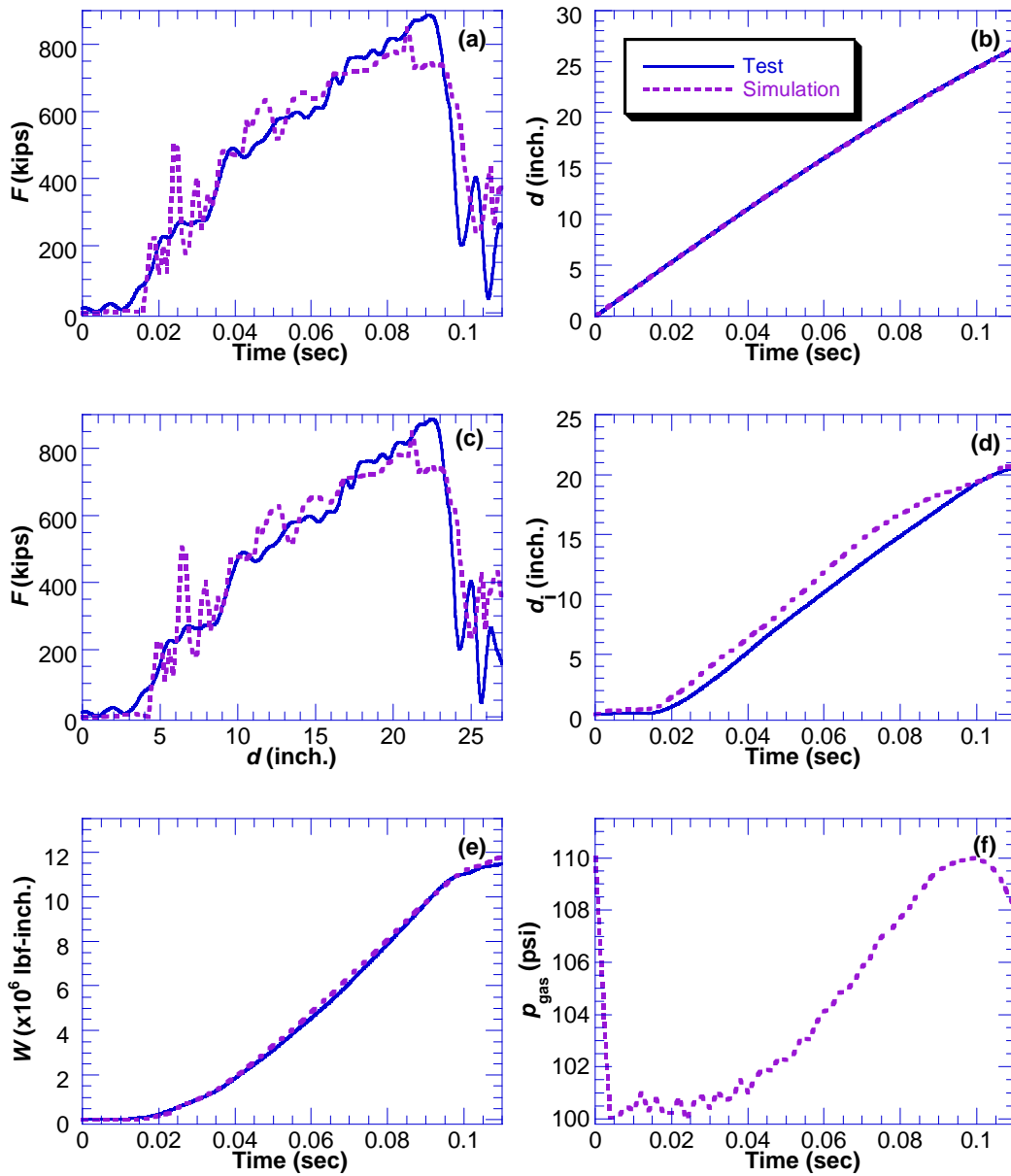


Figure 10. Analysis vs. test results for shell impact Test 2: (a) impact force  $F$ , (b) impactor displacement  $d$ , (c)  $F$ - $d$  cross plot, (d) tank indentation  $d_i$ , (e) work  $W$  done by impact force, and (f) gas pressure  $p_{\text{gas}}$  (analysis data only).

## 6. References

1. Abaqus Inc., Abaqus Analysis User's Manual, Version 6.7.
2. Coltman, M., and M. Hazel, "Chlorine Tank Car Puncture Resistance Evaluation," Final Report, DOT/FRA/ORD-92/11, 1992.
3. Larson, W.G., "Aluminum/Cold Temperature Tank Car Puncture Resistance Tests: Data Report," Final Report, DOT/FRA/ORD-92/29, 1992.
4. Lee, Y.-W., and T. Wierzbicki, "Quick Fracture Calibration for Industrial Use," Impact & Crashworthiness Laboratory, Massachusetts Institute of Technology, Report No: 115, August 2004.
5. Phillips, E.A., and L. Olsen, "Final Phase 05 Report on Tank Car Head Study," RPI-AAR Tank Car Safety Research and Test Project, Report RA-05-1-17, 1972.
6. Ramberg, W., and W.R. Osgood, "Description of Stress-Strain Curves by Three Parameters," National Advisory Committee for Aeronautics, Technical Note No. 902, 1943.
7. Tang, Y.H., Yu, H., Gordon, J.E., Priante, M., Jeong, D.Y., Tyrell, D.C., Perlman, A.B., "Analysis of Full-Scale Tank Car Shell Impact Tests," Proceedings of the 2007 ASME Rail Transportation Division Fall Technical Conference, RTDF2007-46010, September 2007.
8. Tyrell, D.C., Jeong, D.Y., Jacobsen, K., Martinez, E., "Improved Tank Car Safety Research," Proceedings of the 2007 ASME Rail Transportation Division Fall Technical Conference, RTDF2007-46013, September 2007.
9. Yu, H., Jeong, D.Y., Gordon, J.E., Tang, Y.H., "Analysis of Impact Energy to Fracture Unnotched Charpy Specimens Made from Railroad Tank Car Steel," Proceedings of the 2007 ASME Rail Transportation Division Fall Technical Conference, RTDF2007-46038, September 2007.
10. Yu, H., Tang, Y.H., and Jeong, D.Y., "Elastic-Plastic-Failure Finite Element Analyses of Railroad Tank Car Heads in Impact," Proceedings 2007 Abaqus Users' Conference, Paris, France, May 2007.

## 7. Acknowledgement

The Federal Railroad Administration's Office of Research and Development sponsored the research presented in this paper. The full-scale shell impact tests described in this paper were funded and conducted by the Next Generation Rail Tank Car Project which was sponsored by Dow Chemical Company, Union Pacific Railroad, and Union Tank Car Company. FRA participated in this project through a Memorandum of Cooperation.